

CAE-Net: Generalized Deepfake Image Detection using Convolution and Attention Mechanisms with Spatial and Frequency Domain Features

Anindya Bhattacharjee^{DOI a}, Kaidul Islam^{DOI a}, Kafi Anan^{DOI a}, Ashir Intesher^{DOI a}, Abrar Assaeem Fuad^{DOI a}, Utsab Saha^{DOI a,b}, Hafiz Imtiaz^{DOI a}

^a*Department of Electrical and Electronic Engineering, BUET, Dhaka, 1205, Bangladesh*

^b*School of Data and Sciences, BRAC University, Dhaka, 1212, Bangladesh*

Abstract

Effective deepfake detection tools are becoming increasingly essential to the growing usage of deepfakes in unethical practices. There exists a wide range of deepfake generation techniques, which makes it challenging to develop an accurate universal detection mechanism. The 2025 IEEE Signal Processing Cup (*DFWild-Cup* competition) provided a diverse dataset of deepfake images containing significant class imbalance. The images in the dataset are generated from multiple deepfake image generators, for training machine learning model(s) to emphasize the generalization of deepfake detection. To this end, we proposed a disjoint set-based multistage training method to address the class imbalance and devised an ensemble-based architecture *CAE-Net*. Our architecture consists of a convolution- and attention-based ensemble network, and employs three different neural network architectures: EfficientNet, Data-Efficient Image Transformer (DeiT), and ConvNeXt with wavelet transform to capture both local and global features of deepfakes. We visualize the specific regions that these models focus on for classification using Grad-CAM, and empirically demonstrate the effectiveness of these models in grouping real and fake images into cohesive clusters using t-SNE plots. Individually, the EfficientNet B0 architecture has achieved 90.79% accuracy, whereas the ConvNeXt and the DeiT architecture have achieved 89.49% and 89.32% accuracy, respectively. With these networks, our weighted ensemble model achieves an excellent accuracy of 94.63% on the validation dataset of the SP Cup 2025 competition. The equal error rate of 4.72% and the Area Under the ROC curve of 97.37% further confirm the stability of our proposed method. Finally, the robustness of our proposed model against adversarial

perturbation attacks is tested as well, showing the inherent defensive properties of the ensemble approach.

Keywords: Deepfake detection, ConvNext, Transformer, DeiT, Wavelet, EfficientNet

1. Introduction

Deepfakes are media that are edited or created by generative Artificial Intelligence (AI), which do not exist or have not occurred in reality. Although deepfakes have existed for a long time, it took experts, and often entire studios, to generate *convincing* fake media. Due to the surge of machine learning and generative AI tools, the generation of deepfakes has never been easier and more accessible. Such ease of access has raised serious societal concerns since these are being used to manipulate public opinion, commit fraud, create non-consensual pornography, and attack individuals through defamation or identity threats [1]. Deepfakes are also being used to gain malicious political advantage worldwide [2]. Although deepfake generation tools are widely accessible, detection tools are not nearly as effective and accurate. Thus, effective detection of deepfakes is a task of great importance and has been extensively studied for the past decade.

The combination of multiple deep learning architectures has been shown to perform well on deepfake detection. Gowda and Thillaiarasu [3] showed that ensemble techniques of Convolutional Neural Network (CNN) models (ResNeXt and Xception) achieve higher accuracy on deepfake detection. Wodajo and Atnafu [4] combined VGG-16 for feature extraction and Vision Transformer (ViT) for classification, showing promising results on the DFDC dataset. Wolter et al. [5] proposed a wavelet-packet-based analysis for detecting GAN-generated images, highlighting spatial frequency differences in synthetic content and achieving competitive results using combined architectures of wavelets and CNNs. Ricker et al. [6] proposed the usage of frequency domain features extracted via DCT, and achieved high accuracy rates (97.7% for GAN and 73% for diffusion models), highlighting the utility of frequency-domain artifacts. Patel et al. developed an enhanced deep CNN (D-CNN) architecture for deepfake detection, achieving reasonable accuracy and high generalization capability [7]. Patch-Forensics, a technique analyzing smaller patches to detect local image artifacts, achieves 100% average precision on StyleGAN-generated images using an Xception Block 2

classifier [8]. However, Abdullah et al. [9] highlighted two major limitations of the existing networks arguing that the state-of-the-art models often lack control over content and image quality, making them ineffective at detecting high-quality deepfakes if trained on low-quality fake images, and they also lack adversarial evaluation, where an attacker can exploit knowledge of the defense. Works on adversarial perturbation attacks to fool deep neural network (DNN) based detectors are a challenge in deepfake detection [10, 11]. Training on diverse and adversarially perturbed datasets can increase the robustness of a detection architecture [12]. Lin et al. proposed a CNN-based method for deepfake detection that combines multi-scale convolution with a vision transformer [13]. Their approach features a multi-scale module incorporating dilation convolution and depth-wise separable convolution. This design aims to capture more facial details and identify tampering artifacts at various scales [13]. Note that the ViT has gained significant popularity in recent years for deepfake image detection [14, 15].

Researchers are not only relying on complex network architectures but also exploring other approaches, such as the Frequency Enhanced Self-Blending Images (FSBI) method for deepfake detection, which utilizes the Discrete Wavelet Transform (DWT) [16]. Zhu et al. introduced a learnable Image Decomposition Module (IDM) that uses a recombination operation to highlight illumination inconsistencies [17]. It features a multi-level enhancement technique for effective feature recombination and is trained in the logarithmic domain, with an extensible design [17]. To address challenges with low-quality datasets and inadequate detection performance, Cheng et al. have developed MSIDSNet [18]. This framework utilizes a multi-scale fusion (MSF) module to capture forged facial features and an interactive dual-stream (IDS) module to enhance feature integration across frequency and spatial domains [18]. Another recent detection model by Byeon et al. uses a spatial-frequency joint dual-stream convolutional neural network with learnable frequency-domain filtering kernels [19].

Research gap and our contribution. The existing detection methods only work well when the test image resembles the features of the images in the training dataset of the detector. That is, the major issues in the existing detection approaches are i) the lack of generalizability of extracted features and as such, ii) the inability to be up to date with new fake image generation techniques [20]. To address the research gap, the *DFWild-Cup* competition called for novel approaches that can achieve accurate deepfake detection

and provided a diverse dataset (consisting of samples from eight different standard datasets) to help train a generalized deepfake detection algorithm. Such a diverse dataset poses unique challenges to formulating accurate image detection methods. In our proposed solution for generalized deepfake image detection, we have employed a weighted ensemble approach, *CAE-Net*, which utilizes three different neural network architectures with different strengths: i) an EfficientNet architecture, ii) a Data Efficient Image transformer model, and iii) a ConvNeXt model. More specifically, we consolidate the outputs from these architectures and employ a weighted ensemble mechanism to get the final result. We note that the EfficientNet-based architecture, due to its depthwise separable convolution and squeeze and excitation block, allows learning fine spatial artifacts and enhances channel-wise attention [21]. Besides, the self-attention mechanism and the distillation token introduced in the DeiT model allow learning long-range dependencies across the entire image. More specifically, the EfficientNet model excels at capturing local spatial relationships of an image, while the transformer model can capture global features of an image through the self-attention mechanism [22]. Finally, the ConvNeXt model, combined with wavelet transform as a pre-processing technique, is effective in detecting fine-grained artifacts in deepfake images. We have utilized the “Haar” wavelets due to their notable ability to detect abrupt transitions and edges in the data [23]. A weighted ensemble mechanism of these three networks is used as the final solution, which has enabled us to achieve superior performance compared to the models operating alone. Finally, we test our models against adversarial perturbation attacks, which shows the trade-offs between weighted ensemble and majority voting ensemble methods.

The rest of the paper is organized as follows: Section 2 contains data pre-processing techniques, the description of our CAE-Net architecture, consisting of EfficientNet, DeiT, and ConvNeXt. Section 3 contains the accuracy results of multiple standard models on the dataset, along with the implementation details and other evaluation metrics of our proposed approach. This also contains a comparison of our model’s generalization capabilities against multiple existing works and a defense against adversarial perturbations. Finally, Section 4 draws concluding remarks on the contributions presented in the paper.

2. Proposed Methodology: Weighted Ensemble of Neural Network Models

2.1. Description of the Dataset

As mentioned before, the *DFWild-Cup* competition has provided a diverse dataset. The dataset contains images from eight publicly available standard datasets designed for the DeepfakeBench evaluation [24]: Celeb-DF-v1 [25], Celeb-DF-v2 [25], FaceForensics++ [26], DeepfakeDetection [27], FaceShifter [28], UADFV [29], Deepfake Detection Challenge Preview [30], and Deepfake Detection Challenge [31]. To ensure that the detector performance is not biased by specific pre-processing techniques, all datasets underwent uniform pre-processing. Additionally, any information that would identify the origin of the dataset has been eliminated, and the file names have been anonymized. For training, there are a total of 42,690 real images and 219,470 fake images. The validation dataset consists of 1,548 real images and 1,524 fake images. It is evident that there is a significant class imbalance present in the training data, as the ratio of fake and real images is approximately 5:1.

2.2. Data Preprocessing

2.2.1. Class Balancing for Model Training

One of the key contributions of our paper is to devise a disjoint set-based multistage training approach to address the class imbalance present in the given dataset. Since the number of fake images is approximately five times the number of real images, we divided the fake images $\{\mathcal{F}\}$ into five disjoint subsets $\{\mathcal{F}_1, \dots, \mathcal{F}_5\}$. Each of the three aforementioned models, denoted as M_1, M_2, M_3 , are trained in five stages with these disjoint subsets of fake images. At each stage i , the model is trained using the entire real image set \mathcal{R} and one subset of fake images \mathcal{F}_i , such that the training dataset of stage i is given by:

$$\mathcal{D}_i = \mathcal{R} \cup \mathcal{F}_i, \quad i \in \{1, 2, 3, 4, 5\}. \quad (1)$$

We emphasize that the same set of real images $\{\mathcal{R}\}$ are treated as one class during each stage. The training of each model is initialized with pre-trained weights θ_0 , obtained from an ImageNet [32]-trained version of the corresponding architecture. The model parameters at each stage are updated iteratively using the dataset \mathcal{D}_i , through the optimization:

$$\theta_i = \arg \min_{\theta} \sum_{(x,y) \in \mathcal{D}_i} \mathcal{L}(M(x; \theta), y), \quad (2)$$

where \mathcal{L} represents the chosen loss function. After training on \mathcal{D}_i , the final weights θ_i from each stage are used to warm-start the next stage:

$$\theta_{i+1} \leftarrow \theta_i, \quad \text{for } i \in \{1, 2, 3, 4\}. \quad (3)$$

This process continues until the model has been trained on all subsets of fake images, ensuring that the model learns from diverse variations of the fake images while preserving knowledge of real images.

2.2.2. Data Augmentation and Normalization

As mentioned before, we utilized the same set of real images across five training stages to address the class imbalance. However, this evidently increases the chance of overfitting. To mitigate overfitting and enhance the model’s generalization performance, we implemented four data augmentation techniques: random horizontal flips (with 50% probability), random rotations (within $0^\circ - 10^\circ$), color jittering (20% variation in brightness, contrast, saturation and hue), and random resized cropping where it produced 224×224 images, while randomly scaling the crop area between 80% and 120% of the original image size. These augmentations enhanced the diversity of the training dataset, reduced overfitting, and improved the model’s ability to generalize across a wider range of deepfake detection scenarios. It should be noted that such augmentations were used only in training the DeiT architectures. For the ConvNeXt, we employed wavelet transform-based feature extraction from the raw images, and data augmentation techniques would result in incorrect feature representation in the spectral domain. Since all three models were pre-trained using the ImageNet dataset, the training images were normalized using the mean and standard deviation of the ImageNet dataset [32]. The input images were resized accordingly to the specific dimensions for the respective architectures.

2.3. Wavelet Feature Extraction for ConvNeXt

The wavelet transform is shown to be effective for image feature extraction as it decomposes images into multi-resolution frequency components [33]. The ability to decompose an image into different frequency sub-bands while preserving spatial relationships makes it particularly effective at identifying edges, textures, and subtle patterns of an image [34]. Using 2D Wavelet transform, an image can be decomposed into *approximate* and *detail* coefficients [23]. As such, we performed a single-level 2D Discrete Wavelet

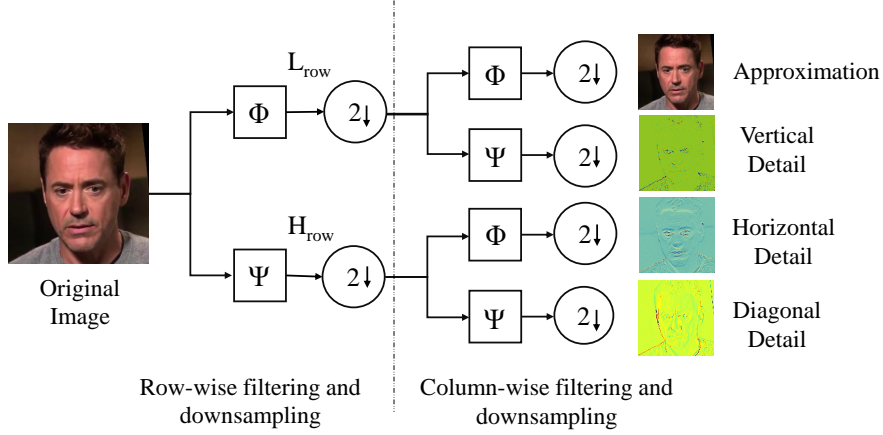


Figure 1: Row- and column-wise filtering and downsampling to generate approximation and detail images through 2D-Discrete Wavelet Transform (DWT) using Haar wavelets.

Transform (2D-DWT) using Haar wavelets to produce the approximate and detailed coefficients of the images and used the computed coefficients as features.

The 2D-DWT is applied to an image $I(x, y)$ to decompose it into frequency sub-bands while preserving spatial information. Given an image $I \in \mathbb{R}^{M \times N}$, a single-level 2D-DWT using Haar wavelets generates four coefficient matrices: the approximate coefficients and three sets of detail coefficients (horizontal, vertical, and diagonal). The wavelet decomposition is performed using separable filtering along rows and columns. The Haar wavelet uses two filters:

- **Low-pass filter (ϕ):** Coefficients $\left[\frac{1}{\sqrt{2}}, \frac{1}{\sqrt{2}} \right]$
- **High-pass filter (ψ):** Coefficients $\left[-\frac{1}{\sqrt{2}}, \frac{1}{\sqrt{2}} \right]$

As shown in Figure 1, the sub-bands are computed as follows:

1. Row-wise filtering and downsampling:

$$L_{\text{row}} = (I * \phi) \downarrow_{2, \text{cols}}$$

$$H_{\text{row}} = (I * \psi) \downarrow_{2, \text{cols}}$$

2. Column-wise filtering and downsampling:

$$\begin{aligned}
 A &= (L_{\text{row}} * \phi) \downarrow_{2,\text{rows}} && \text{(Approximation, LL)} \\
 V &= (L_{\text{row}} * \psi) \downarrow_{2,\text{rows}} && \text{(Vertical Details, LH)} \\
 H &= (H_{\text{row}} * \phi) \downarrow_{2,\text{rows}} && \text{(Horizontal Details, HL)} \\
 D &= (H_{\text{row}} * \psi) \downarrow_{2,\text{rows}} && \text{(Diagonal Details, HH),}
 \end{aligned}$$

where $*$ indicates convolution; $\downarrow_{2,\text{cols}}$ and $\downarrow_{2,\text{rows}}$ indicate downsampling the columns and rows by 2, respectively; A denotes low-frequency approximation coefficients; and H, V, D denote high-frequency horizontal, vertical, and diagonal detail coefficients, respectively. For an RGB image I_r, I_g, I_b consisting of three color channels, we apply the above transformation independently to each color channel:

$$A_c, H_c, V_c, D_c = \text{DWT}(I_c), \quad c \in \{r, g, b\}, \quad (4)$$

where A_c, H_c, V_c, D_c are the approximate and detail coefficients for each color channel c . The final feature representation is formed by concatenating the coefficients across all three channels:

$$F = \text{concat}((A_r, A_g, A_b), (H_r, H_g, H_b), (V_r, V_g, V_b), (D_r, D_g, D_b)). \quad (5)$$

To prepare the wavelet-domain features for classification, the coefficients are scaled to an 8-bit integer range and resized to match the input dimensions of the ConvNeXt model. In Figure 2, we showed two such feature images with the approximate and detailed coefficients of two sample images from the dataset.

2.4. Details of the Model Architectures

Recall that our proposed solution utilizes three neural network models for a weighted ensemble approach for our final prediction. We chose each of these models to focus on different aspects of a deepfake image so that the ensemble approach provides better accuracy than individual models operating alone. The details of the models in our proposed solution are presented below.

2.4.1. EfficientNet

EfficientNet-B0 is a computationally efficient model whose architecture is optimized via neural architecture search (NAS) to maximize accuracy under a FLOP constraint, resulting in a highly efficient baseline that outperforms

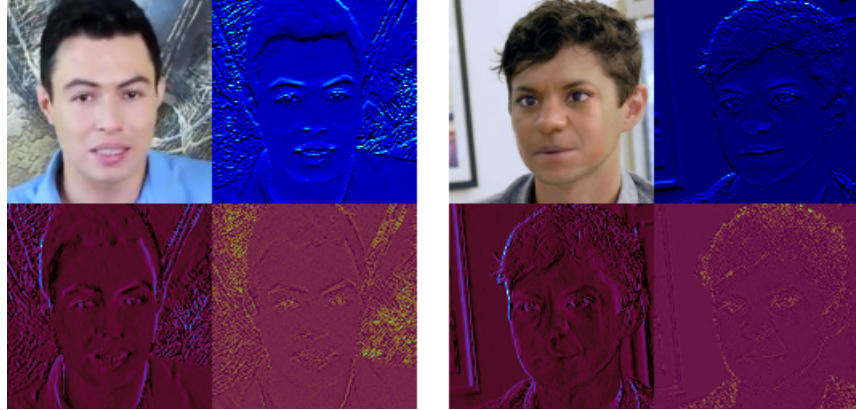


Figure 2: Real and Fake feature images after wavelet transform. The top left, top right, bottom left, and bottom right portions indicate the approximate, horizontal detail, vertical detail, and diagonal detail coefficients of the original image, respectively. Different colormaps are applied to the horizontal, vertical, and diagonal detail coefficients, and their contrasts are increased for better visibility.

models with similar computational cost [21]. The core block of the EfficientNet architecture is the Mobile Inverted Bottleneck Convolution (MBConv) block inspired by MobileNetV2 [35].

The MBConv block consists of a 1x1 Convolution, which expands the input channels to increase feature dimensionality. Then, a 3x3 or 5x5 depthwise convolution is applied to capture spatial features efficiently. Squeeze-and-Excitation (SE) recalibrates channel importance by computing a channel-wise attention vector [36]. The SE block acts as a lightweight attention mechanism to adaptively recalibrate each feature channel’s importance [37]. It is responsible for two main operations:

Squeeze: Global spatial information is aggregated using global average pooling to generate channel-wise descriptors. Given an input feature map $X \in \mathbb{R}^{H \times W \times C}$, the squeezed feature vector $z \in \mathbb{R}^C$ is obtained by squeezing function $F_{sq}(.)$ as:

$$z_c = \frac{1}{HW} \sum_{i=1}^H \sum_{j=1}^W X_c(i, j), \quad c = 1, 2, \dots, C, \quad (6)$$

where $X_c(i, j)$ represents the activation at spatial location (i, j) in channel c .

Excitation: The descriptors generated from the Squeeze block are passed through a lightweight two-layer fully connected network with a bottleneck

Table 1: Summary of the EfficientNetB0 Model Architecture

| Layer (type) | Output Shape | Param # |
|-------------------------------|----------------|-----------|
| Conv2D + BatchNorm + SiLU | [32, 112, 112] | 928 |
| DepthwiseSeparableConv | [16, 112, 112] | 1,448 |
| InvertedResidual-1 \times 2 | [24, 56, 56] | 16,714 |
| InvertedResidual-2 \times 2 | [40, 28, 28] | 46,640 |
| InvertedResidual-3 \times 3 | [80, 14, 14] | 242,930 |
| InvertedResidual-4 \times 3 | [112, 14, 14] | 543,148 |
| InvertedResidual-5 \times 4 | [192, 7, 7] | 2,026,348 |
| InvertedResidual-6 | [320, 7, 7] | 717,232 |
| Conv2d + BatchNorm + SiLU | [1280, 7, 7] | 412,160 |
| AdaptiveAvgPool2d + Flatten | [1280] | 0 |
| Linear | [1] | 1,281 |
| Total Parameters | | 4,008,829 |
| Trainable Parameters | | 4,008,829 |
| Non-Trainable Parameters | | 0 |

structure to model non-linear channel independencies.

After that, a skip connection adds the input to the output if the input and output shapes match. The swish activation [38] function is applied after each convolution except the final projection.

$$\text{Swish}(x) = x \cdot \sigma(x) = \frac{x}{1 + e^{-x}} \quad (7)$$

EfficientNet-B0 uses MBConv1 (expansion factor 1) to MBConv6 (expansion factor 6) variants, with kernel sizes of 3x3 or 5x5 depending on the stage. A brief summary of different layers, the output shapes and the number of parameters in the EfficientNet-B0 architecture is shown in Table 1.

2.4.2. Data Efficient Image Transformer (DeiT)

Unlike conventional Recurrent Neural Networks (RNNs), transformers process all inputs simultaneously, relying on a self-attention mechanism. This allows transformers to learn long-range dependencies and global contexts of data [22]. The data-efficient image transformer, based on the backbone of the vision transformer, has been shown to work well in cases where training data is limited [39]. Here, an image is divided into a grid of smaller patches as a sequence of input tokens (N number of 16×16 patches), and each

patch is associated with a vector through linear embedding. After adding positional encoding for each patch, the vectors are fed into the transformer encoder, where the self-attention mechanism helps to learn the relationship among all the patches [40]. Note that the attention mechanism is based on a trainable associative memory of (key, value) pairs. A query vector \mathbf{Q} is matched against key vectors $\{\mathbf{K}\}$ using dot products, scaled by \sqrt{d} , and normalized via a softmax function to produce weights. These weights are used to compute a weighted sum of value vectors $\{\mathbf{V}\}$, producing an output matrix as:

$$\text{attention}(\mathbf{Q}, \mathbf{K}, \mathbf{V}) = \text{softmax}\left(\frac{\mathbf{Q}\mathbf{K}^\top}{\sqrt{d}}\right)\mathbf{V} \quad (8)$$

In self-attention, the queries, keys, and values are derived from the same input sequence via linear transformations [41]. Multi-head self-attention (MSA) applies h separate attention functions (heads) in parallel. Each head provides a sequence of outputs, which are concatenated and projected back to the original dimension. This allows the model to attend to different parts of the input sequence simultaneously.

DeiT is an effective alternative to traditional CNNs in learning global features [22], using knowledge distillation techniques and optimization strategies to improve generalization. DeiT learns from a pre-trained CNN model (that is, the RegNetY-16GF model [42]) and uses a distillation token during training, allowing it to learn faster and more efficiently with less data [39].

The DeiT architecture introduces a new hard distillation mechanism where they treat the hard decisions of the teacher model y_t as true labels along with the actual true labels, y . If Z_t are the logits of the teacher model and Z_s are the logits of the student model, then the hard decision of the teacher model is defined as

$$y_t = \text{argmax}_c(Z_t(c)) \quad (9)$$

Here, c is the class index. Using this prediction, the final loss function for hard distillation is treated as

$$L_{\text{global dist}}^{\text{hard dist}} = \frac{1}{2}L_{CE}(\text{softmax}(Z_s), y) + \frac{1}{2}L_{CE}(\text{softmax}(Z_s), y_t) \quad (10)$$

The first term of the equation can be thought of as $L_{\text{cross-entropy}}$ and the second term as L_{teacher} .

Our proposed solution utilizes the DeiT-B model, a 768-dimensional model with 12 heads and 86 million parameters, based on the ViT-B model [39].

Table 2: Summary of the Data Efficient Image Transformer (DeiT) Model Architecture

| Layer (type) | Output Shape | Param # |
|------------------------------------|---------------|------------|
| Conv2d | [764, 14, 14] | 590,592 |
| Patch Embed | [196, 768] | 0 |
| Dropout + Identity-1 | [197, 768] | 0 |
| LayerNorm \times 25 | [197, 768] | 38,400 |
| Linear-1 \times 12 | [197, 2304] | 21,261,312 |
| Identity-2 | [12, 197, 64] | 0 |
| (Linear-2 + Attention) \times 12 | [197, 768] | 35,407,872 |
| (Linear-3 + GELU) \times 12 | [197, 3072] | 28,348,416 |
| Dropout | [197, 3072] | 0 |
| Mlp \times 12 | [197, 768] | 0 |
| Identity and Dropout | [768] | 0 |
| Linear-4 | [2] | 1,538 |
| Vision Transformer | [2] | 0 |
| Total Parameters | | 85,648,130 |
| Trainable Parameters | | 85,648,130 |
| Non-Trainable Parameters | | 0 |

The summary number of parameters and the output shapes of layers are shown in Table 2.

2.4.3. ConvNeXt Model

ConvNeXt combines the efficiency and inductive biases of traditional CNNs with the scalability and performance of transformers. It employs an inverted bottleneck block, similar to transformers’ MLP blocks, reducing FLOPs in downsampling layers. Here, batch normalization is replaced with layer normalization, aligning with transformer practices, and GELU is used instead of ReLU for smoother non-linearity [43].

Inspired by both ResNets [44] and Swin transformers [45], the architecture includes a patchify stem where input images are processed by a 4x4 convolution with stride 4, followed by layer normalization, to downsample the image into non-overlapping patches. This mimics ViT’s patch embedding but uses convolutions.

Each ConvNeXt block contains a 7x7 depthwise convolution (one filter per input channel) that is applied to capture spatial features efficiently. Then layer normalization is applied before and after the convolution to stabilize

training. It normalizes features across the channel dimension for each spatial position. For feature $X[i, j, :] \in \mathbf{R}^C$ the normalized output is:

$$\hat{X}[i, j, c] = \frac{X[i, j, c] - \mu}{\sqrt{\sigma^2 + \epsilon}} \cdot \gamma + \beta \quad (11)$$

Here $\mu = \frac{1}{C} \sum_{c=1}^C X[i, j, c]$, $\sigma^2 = \frac{1}{C} \sum_{c=1}^C (X[i, j, c] - \mu)^2$, ϵ is a small constant, and γ and β are trainable parameters. This type of normalization works better than typical batch normalization [46]. After that, pointwise convolution is applied to expand (to 4x the input dimension) and contract the feature map, mimicking transformer MLP layers. GELU (Gaussian Error Linear Unit) [47] is applied instead of RELU for smoother non-linearity.

$$\text{GELU}(x) = x \cdot \Phi(x) = x \cdot \frac{1}{2} [1 + \text{erf}(\frac{x}{\sqrt{2}})] \quad (12)$$

A skip connection is used from the input to the block’s output, similar to ResNet’s residual connections [44]. Between stages, ConvNeXt uses a down-sampling layer with layer normalization and a 2x2 convolution with stride 2, inspired by Swin Transformer’s separate downsampling strategy, unlike ResNet’s within-block downsampling. From the diverse family of ConvNeXt architectures, we specifically implemented the ConvNeXt-tiny model for its low compute and high accuracy on the dataset. A summary of the different layers in the ConvNeXt-tiny architecture that we have implemented is presented in Table 3.

2.4.4. Proposed Weighted Ensemble Architecture: CAE-Net

Finally, we implemented a weighted ensemble mechanism to combine the predictions of the aforementioned three models. The associated weights for the EfficientNet, DeiT, and ConvNeXt with wavelet transform are 0.35, 0.34, and 0.31, respectively, based on our parameter search. The final architecture is shown in Figure 3.

2.5. Adversarial Perturbations

Adversarial perturbations are crafted noises or modifications added to classifier model inputs, often imperceptible to humans, that can significantly deteriorate model performance and lead to misclassification. Such adversarial perturbations can be universal or image-dependent [48] and are usually

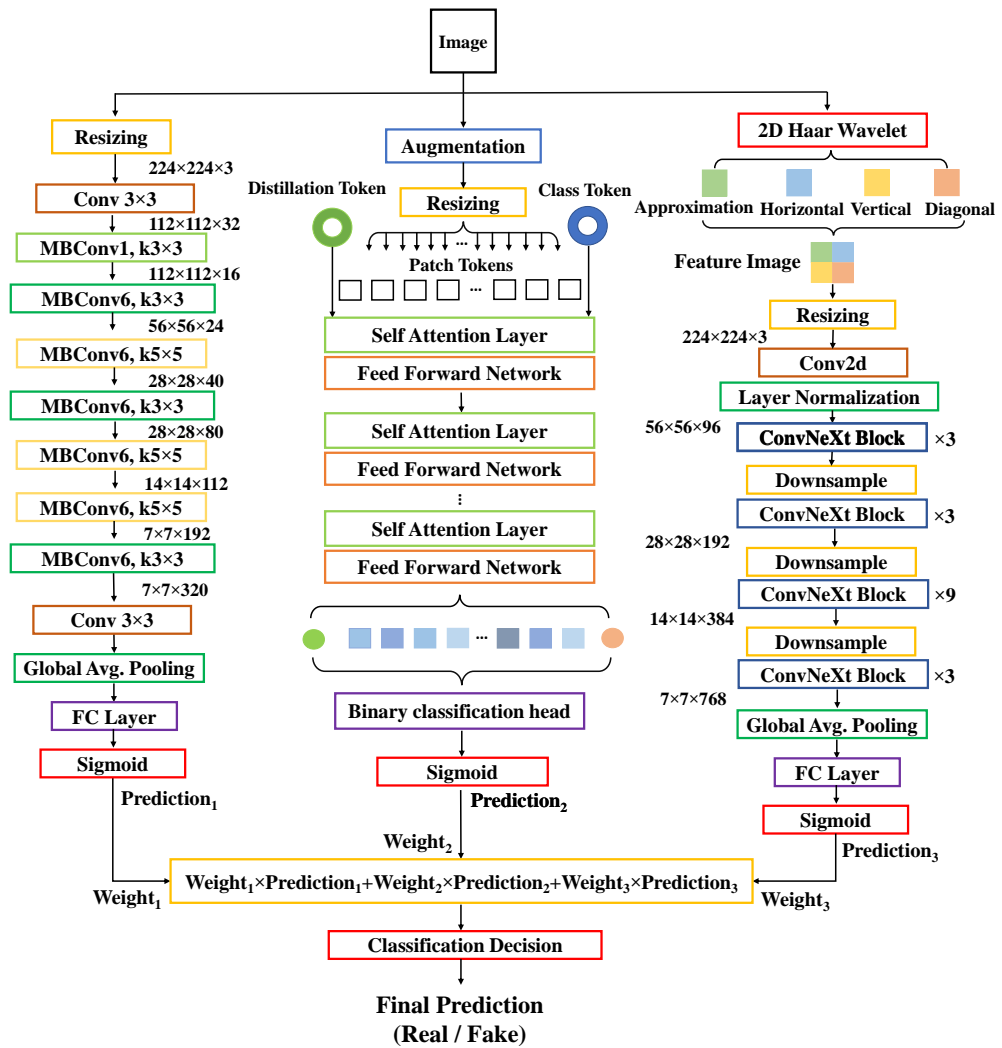


Figure 3: The proposed CAE-Net architecture

Table 3: Summary of the ConvNeXt Architecture

| Layer Type | Output Shape | Param # |
|---------------------------------|---------------|------------|
| Conv2d + LayerNorm2d | [96, 74, 74] | 4,896 |
| CNBlock ($\times 3$) | [96, 74, 74] | 237,600 |
| LayerNorm2d + Conv2d | [192, 37, 37] | 74,112 |
| CNBlock ($\times 3$) | [192, 37, 37] | 917,568 |
| LayerNorm2d + Conv2d | [384, 18, 18] | 295,680 |
| CNBlock ($\times 9$) | [384, 18, 18] | 10,813,824 |
| LayerNorm2d + Conv2d | [768, 9, 9] | 1,181,184 |
| CNBlock ($\times 3$) | [768, 9, 9] | 14,287,104 |
| AdaptiveAvgPool2d + LayerNorm2d | [768, 1, 1] | 1536 |
| Flatten + Linear | [1] | 769 |
| Total Parameters | | 27,814,273 |
| Trainable Parameters | | 27,814,273 |
| Non-Trainable Parameters | | 0 |

done in white-box settings where access to the model’s architecture and parameters is required. Also, adversarial attacks on a known network have been shown to work effectively against other networks as well [49], making black-box attacks an imminent threat for sensitive issues like deepfake detection [50]. We evaluate the robustness of our proposed models by testing them against a simple but effective adversarial perturbation, the Fast Sign Gradient Method (FGSM). FGSM is a white-box attack without specifying a target class. Using this method, adversarial images are created by calculating the gradient of loss for input data and adjusting the input by a small amount in the direction of the gradient sign [49].

$$x_{\text{adv}} = x + \epsilon \cdot \text{sign}(\nabla_x J(\theta, x, y)) \quad (13)$$

Here (x, y) are the original input image and its label, θ indicates model parameters, x_{adv} is the adversarially perturbed image, and $\nabla_x J(\theta, x, y)$ is the gradient of the loss function J with respect to the input image x . The parameter ϵ controls the magnitude of the perturbation added to the original image. This method works like a gradient ascent algorithm trying to maximize the loss with the smallest possible perturbation, ϵ , which makes it barely noticeable to the human eye. Though FGSM is one of the simplest forms of perturbations, it has been shown to reduce the accuracy of high-quality detectors to a large extent [51]. Its effectiveness for binary classification

problems makes it an ideal choice for testing the robustness of our proposed method.

3. Experimental Results

In this section, we demonstrate the performance of our proposed solution on the competition dataset. No prior work exists on this novel combined deepfake image detection dataset, which consists of images from eight different benchmark deepfake video datasets. To address this, we hypothesized that lightweight CNNs(e.g., EfficientNet) would excel in resource-constrained settings, modern CNNs (e.g., ConvNeXt) would leverage transformer-inspired designs for better feature extraction, and ViTs would capture the global context of images. We systematically evaluated these models to test these hypotheses along with multiple other frequency domain feature extraction techniques, establishing the first performance benchmarks for the dataset.

Hyperparameters. For the training of our models, we have used the ADAM optimizer and binary categorical cross-entropy as our loss function. Using the validation set to observe the accuracy of the proposed architecture, each image took approximately 0.03385416s on a Tesla P100 GPU. The hyperparameters used for training are presented in Table 5.

Result Analysis. We evaluated our weighted ensemble model for multiple evaluation metrics, including accuracy, precision, recall, F1-score, area under the receiver operating characteristic (AU-ROC) curve, equal error rate, and average precision. While calculating these metrics, real images were considered as class 0 and fake images as class 1. The performance of our model on these metrics is presented in Table 6 and the confusion matrix and the ROC curve are shown in Figure 4. It is evident from the evaluation indices that our proposed weighted ensemble architecture performs very well on the competition dataset, which underlines the generalization capability of the proposed approach.

To investigate the performance of our ensemble model, we intend to visualize i) the regions of the images that the three models focus on for classification, and ii) how the three models distinguish real and fake images before and after training. To that end, we note that the Grad-CAM visualizations show how different models focus on different facial regions of the same image

Table 4: Comparative Analysis of Different Model Variations

| Classifier Models | Accuracy |
|--|---------------|
| CNN models | |
| VGG-19 [52] | 62.25% |
| ResNet-50 [44] | 69.00% |
| MobileNet-V2 | 78.12% |
| ResNet-34 [44] | 80.32% |
| RegNet [53] | 80.92% |
| Inception V3 [54] | 84.38% |
| ResNet-34 with CBAM | 85.19% |
| ResNet-34 with single SE | 88.90% |
| DenseNet-121 [55] | 90.01% |
| EfficientNet-B0 [21] | 90.79% |
| EfficientNet-B4 [21] | 87.27% |
| EfficientNet-B5 [21] | 88.31% |
| ResNeXt [56] | 85.19% |
| ConvNeXt [43] | 88.18% |
| Frequency Domain Experimentations | |
| DCT with ResNet-34 | 71.48% |
| ResNet-34 with Wavelet | 80.44% |
| EfficientNetB0 with Wavelet | 82.48% |
| Xception-Net [57] with Wavelet | 87.76% |
| ConvNeXt with Wavelet | 89.49% |
| Study on Transformers | |
| ViT-B [58] | 78.12% |
| Swin Transformer [45] | 86.52% |
| MobileViT [59] | 87.04% |
| DeiT [39] | 89.32% |
| Ensemble Results | |
| Maj. Voting (EfficientNet, DeiT, ConvNeXt) | 94.24% |
| Proposed Weighted Ensem. (EfficientNet, DeiT, ConvNeXt) | 94.63% |

Table 5: Hyperparameters for model training

| Hyperparameters | Details |
|----------------------------------|--------------------|
| Batch size | 32 |
| Number of Epochs in each session | — |
| - EfficientNet | 5 |
| - DeiT | 5 |
| - ConvNeXt | 4 |
| Learning rate | — |
| - Learning rate scheduler | ReducedLROnPlateau |
| - Initial learning rate | 0.0001 |
| - Reduction factor | 0.1 |
| - Patience | 3 |

Table 6: Performance of the Final Ensemble Architecture combining ConvNext, DeiT, and EfficientNet

| Evaluation Metrics | Performance |
|--------------------|-------------|
| Accuracy | 94.63% |
| Precision | 0.937 |
| Recall | 0.956 |
| F1 score | 0.9464 |
| Area under ROC | 0.9737 |
| Equal Error Rate | 4.72% |
| Average Precision | 0.9771 |

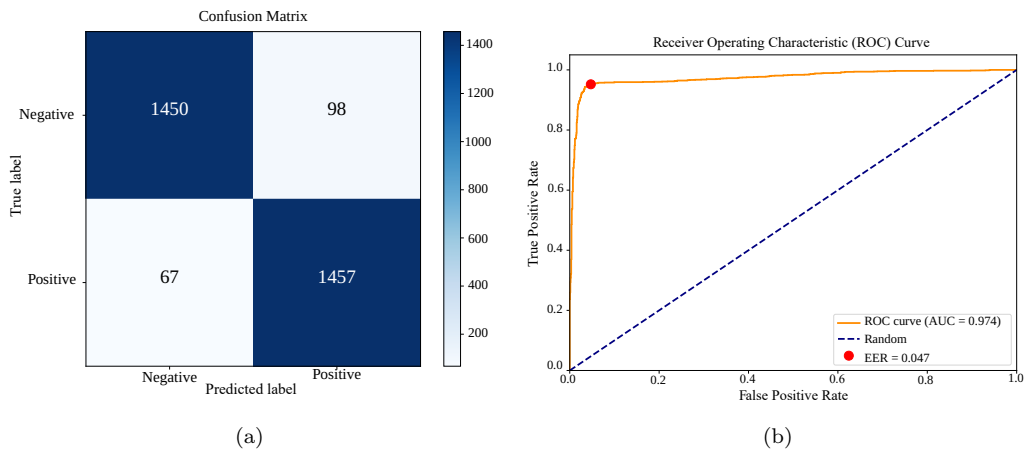


Figure 4: (a) Confusion matrix and (b) ROC curve for validation set

for deepfake detection. In Figure 5, it can be seen that EfficientNet focuses on localized facial features, whereas DeiT displays diffuse attention patterns indicating a focus on global features. When the diverse insights from each model are combined into an ensemble, the overall prediction becomes more accurate, robust, and better at generalizing to new data. Additionally, we present the Grad-CAM view of some of the wrong predictions by the three models in Figure 6, showing the focus of irrelevant regions, leading to misclassifications.

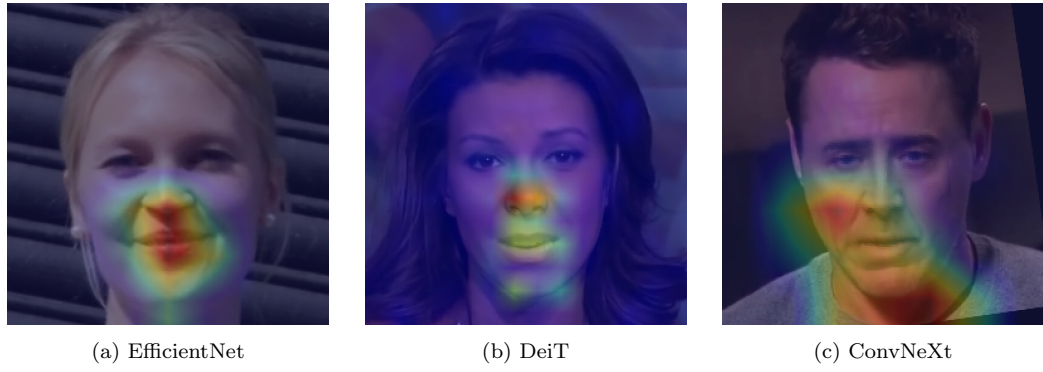


Figure 5: Importance map shown by Grad-CAM for different models



Figure 6: Grad-CAM view of a few failed classifications of our proposed model

Next, we note that high-dimensional data can be visualized by projecting onto a two-dimensional space using the non-linear dimensionality reduction technique known as t-SNE (t-Distributed Stochastic Neighbor Embedding) [60]. By maintaining the local neighborhoods of data points, it shows

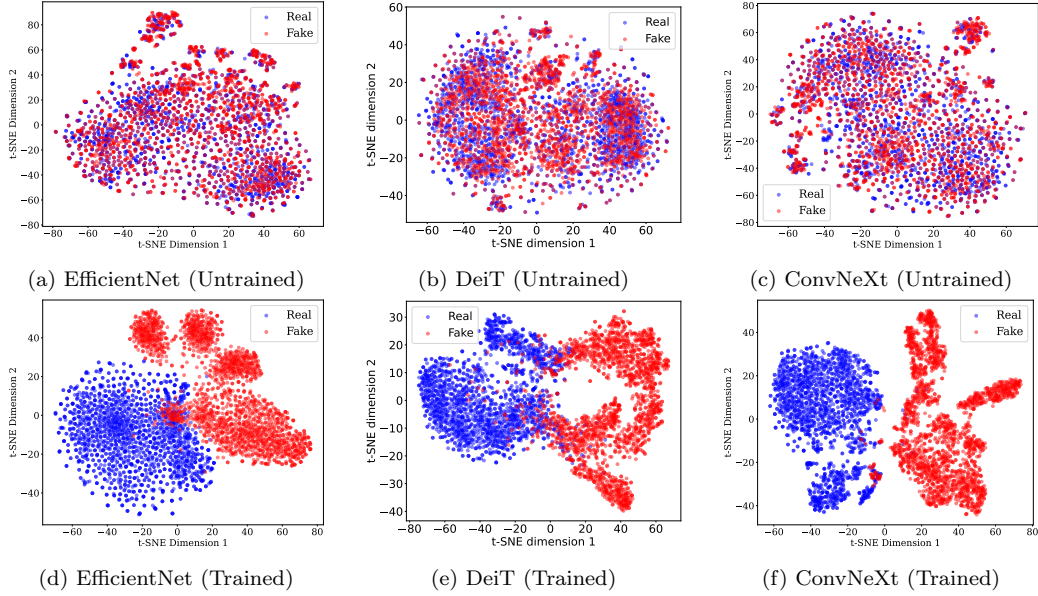


Figure 7: t-SNE plot of three models before and after training for randomly selected 4000 real and fake images using perplexity = 40

the differences and similarities of data points in the learned feature space. As such, the t-SNE visualizations (Fig. 7) offer valuable insights into the effectiveness of our models. For both real and fake images, we observe cohesive clusters for all three models, despite the images being produced using various deepfake generation methods. This highlights the generalization capability of our proposed ensemble model. After training, all three backbone models, i.e., EfficientNet, DeiT, and ConvNeXt, produced well-separated embeddings for real and fake images, as illustrated in Fig. 7d, 7e, and 7f. There exist very few works on deepfake detection that perform well on the combination of such a diverse set of datasets. A comparative analysis among existing works with our proposed architecture is shown in Table 7. Note that the AUC score presented here is the mean score of these models on the corresponding datasets (we refer the reader to Figure 8 of [25]). We want to emphasize that existing works often demonstrate good performance on only a few datasets, but the overall performance on multiple datasets is very poor for most architectures.

Finally, we look into the effectiveness of our ensemble method through a simple adversarial perturbation attack, such as Fast Gradient Sign Method (FGSM). As mentioned before, FGSM can fool models by adding simple

Table 7: Comparative Analysis of Average AUC Score of Different Models

| Detection Method | Datasets | AUC Score | Std. Dev. |
|---------------------|--|---------------|-----------|
| Capsule [61] | UADFV [29], DF-TIMIT [62], FaceForensics++ [26], DFD [27], DFDC [31], Celeb-DF [25] | 69.4% | 13.84% |
| Meso4 [63] | UADFV [29], DF-TIMIT [62], FaceForensics++ [26], DFD [27], DFDC [31], Celeb-DF [25] | 75.9% | 10.63% |
| FWA [64] | UADFV [29], DF-TIMIT [62], FaceForensics++ [26], DFD [27], DFDC [31], Celeb-DF [25] | 82.1% | 14.45% |
| Xception-C23 [26] | UADFV [29], DF-TIMIT [62], FaceForensics++ [26], DFD [27], DFDC [31], Celeb-DF [25] | 86.4% | 11.96% |
| DSP-FWA [25] | UADFV [29], DF-TIMIT [62], FaceForensics++ [26], DFD [27], DFDC [31], Celeb-DF [25] | 87.4% | 12.79% |
| Our Proposed Method | Celeb-DF [25], DFDC [31], DFD [27], UADFV [29], FaceShifter [28], DFDC Preview [30], FaceForensics++ [26] | 97.37% | - |

Table 8: Comparison of Our Proposed Architectures under Adversarial FGSM Attacks

| Model | Accuracy | | |
|--|-------------------|-------------------|-------------------|
| | $\epsilon = 0.01$ | $\epsilon = 0.03$ | $\epsilon = 0.05$ |
| EfficientNetB0 | 38.54% | 46.48% | 53.94% |
| Data Efficient Image Transformer | 42.76% | 21.94% | 16.73% |
| ConvNeXt with wavelet | 6.45% | 6.51% | 15.40% |
| Weighted Ensem.(EfficientNet, DeiT, ConvNeXt) | 12.04% | 13.48% | 16.05% |
| Majority Voting (EfficientNet, DeiT, ConvNeXt) | 25.52% | 20.41% | 19.76% |

perturbation noise based on the gradient sign that intends to maximize the loss function of the detection model instead of minimizing it. We present the accuracy scores of the separate detection model as well as the ensemble models for different values of ϵ in Table 8. The results show an increased robustness of the EfficientNet architecture, which depicts increased accuracy with increasing perturbation compared to the other two architectures. DeiT shows a decrease in accuracy with rising perturbation, and ConvNeXt accuracy drops significantly even for very low perturbation added to the image. Though a weighted ensemble model is appropriate for achieving high accuracy on the generalized dataset, we argue that it is highly vulnerable to adversarial attacks. If any model performs poorly on adversarial data, then the performance of the entire ensemble drops significantly. However, in the majority voting ensemble, the performance does not reduce as much, since it requires the majority of models to perform poorly, implying increased robustness against adversarial attacks for applications, such as deepfake detection.

4. Conclusion

In this work, we proposed an ensemble architecture for deepfake detection that captured the intricate properties of the input images to successfully distinguish between real and fake images and produced excellent results. We emphasize that detecting deepfake images that are generated with a range of generative AI approaches is a challenging task. To that end, we have addressed a significant class imbalance through disjoint training set-based multistage training, and proposed a weighted ensemble approach that takes advantage of the strengths of an EfficientNet model, a Data Efficient Image Transformer model, and a ConvNext model for the accurate classification of deepfake images. The EfficientNet-B0 model enabled extracting local features from an image, while the DeiT model specialized in capturing global features. Additionally, ConvNeXt, combined with the wavelet transform, effectively identified frequency-dependent artifacts. Through t-SNE plots, we demonstrated that our model is capable of separating real and fake images into separable clusters. Additionally, we included Grad-CAM visualizations to map the focus regions of images to illustrate how our models analyze the images and which portions contribute to distinguishing between real and fake images. Besides, we further analyzed the effectiveness of the proposed models by testing them against FGSM attacks and found the optimum ensemble mechanism to be majority voting compared to the weighted ensemble with a little trade-off in accuracy. An interesting future work could be incorporating lightweight architectures, reducing the computational overhead, and increasing the model’s adaptability to newer and sophisticated deepfake generation methods.

References

- [1] V. Karasavva, A. Noorbhai, The real threat of deepfake pornography: A review of canadian policy, *Cyberpsychology, Behavior, and Social Networking* 24 (3) (2021) 203–209.
- [2] M. Westerlund, The emergence of deepfake technology: A review, *Technology innovation management review* 9 (11) (2019).
- [3] A. Gowda, N. Thillaiarasu, Investigation of comparison on modified cnn techniques to classify fake face in deepfake videos, in: 2022 8th

International Conference on Advanced Computing and Communication Systems (ICACCS), Vol. 1, IEEE, 2022, pp. 702–707.

- [4] D. Wodajo, S. Atnafu, Deepfake video detection using convolutional vision transformer, arXiv preprint arXiv:2102.11126 (2021).
- [5] M. Wolter, F. Blanke, R. Heese, J. Garcke, Wavelet-packets for deepfake image analysis and detection, *Machine Learning* 111 (11) (2022) 4295–4327.
- [6] J. Ricker, S. Damm, T. Holz, A. Fischer, Towards the detection of diffusion model deepfakes, arXiv preprint arXiv:2210.14571 (2022).
- [7] Y. Patel, S. Tanwar, P. Bhattacharya, R. Gupta, T. Alsuwian, I. E. Davidson, T. F. Mazibuko, An improved dense cnn architecture for deepfake image detection, *IEEE Access* 11 (2023) 22081–22095.
- [8] J. Frank, T. Eisenhofer, L. Schönherr, A. Fischer, D. Kolossa, T. Holz, Leveraging frequency analysis for deep fake image recognition, in: International conference on machine learning, PMLR, 2020, pp. 3247–3258.
- [9] S. M. Abdullah, A. Cheruvu, S. Kanchi, T. Chung, P. Gao, M. Jadliwala, B. Viswanath, An analysis of recent advances in deepfake image detection in an evolving threat landscape, arXiv preprint arXiv:2404.16212 (2024).
- [10] S. Hussain, P. Neekhara, M. Jere, F. Koushanfar, J. McAuley, Adversarial deepfakes: Evaluating vulnerability of deepfake detectors to adversarial examples, in: Proceedings of the IEEE/CVF winter conference on applications of computer vision, 2021, pp. 3348–3357.
- [11] A. Gandhi, S. Jain, Adversarial perturbations fool deepfake detectors, in: 2020 International joint conference on neural networks (IJCNN), IEEE, 2020, pp. 1–8.
- [12] T. T. Nguyen, Q. V. H. Nguyen, D. T. Nguyen, D. T. Nguyen, T. Huynh-The, S. Nahavandi, T. T. Nguyen, Q.-V. Pham, C. M. Nguyen, Deep learning for deepfakes creation and detection: A survey, *Computer Vision and Image Understanding* 223 (2022) 103525.

- [13] H. Lin, W. Huang, W. Luo, W. Lu, Deepfake detection with multi-scale convolution and vision transformer, *Digital Signal Processing* 134 (2023) 103895.
- [14] Y.-J. Heo, W.-H. Yeo, B.-G. Kim, Deepfake detection algorithm based on improved vision transformer, *Applied Intelligence* 53 (7) (2023) 7512–7527.
- [15] S. Usmani, S. Kumar, D. Sadhya, Efficient deepfake detection using shallow vision transformer, *Multimedia Tools and Applications* 83 (4) (2024) 12339–12362.
- [16] A. A. Hasanaath, H. Luqman, R. Katib, S. Anwar, Fsb: Deepfake detection with frequency enhanced self-blended images, *Image and Vision Computing* (2025) 105418.
- [17] C. Zhu, B. Zhang, Q. Yin, C. Yin, W. Lu, Deepfake detection via inter-frame inconsistency recomposition and enhancement, *Pattern Recognition* 147 (2024) 110077.
- [18] Z. Cheng, Y. Wang, Y. Wan, C. Jiang, Deepfake detection method based on multi-scale interactive dual-stream network, *Journal of Visual Communication and Image Representation* 104 (2024) 104263.
- [19] H. Byeon, M. Shabaz, K. Shrivastava, A. Joshi, I. Keshta, R. Oak, P. P. Singh, M. Soni, Deep learning model to detect deceptive generative adversarial network generated images using multimedia forensic, *Computers and Electrical Engineering* 113 (2024) 109024.
- [20] A. Kaur, A. Noori Hoshyar, V. Saikrishna, S. Firmin, F. Xia, Deepfake video detection: challenges and opportunities, *Artificial Intelligence Review* 57 (6) (2024) 1–47.
- [21] M. Tan, Q. Le, Efficientnet: Rethinking model scaling for convolutional neural networks, in: *International conference on machine learning*, PMLR, 2019, pp. 6105–6114.
- [22] S. Khan, M. Naseer, M. Hayat, S. W. Zamir, F. S. Khan, M. Shah, Transformers in vision: A survey, *ACM computing surveys (CSUR)* 54 (10s) (2022) 1–41.

- [23] P. Porwik, A. Lisowska, The haar-wavelet transform in digital image processing: its status and achievements, *Machine graphics and vision* 13 (1/2) (2004) 79–98.
- [24] Z. Yan, Y. Zhang, X. Yuan, S. Lyu, B. Wu, Deepfakebench: A comprehensive benchmark of deepfake detection, in: *Advances in Neural Information Processing Systems*, Vol. 36, Curran Associates, Inc., 2023, pp. 4534–4565.
- [25] Y. Li, X. Yang, P. Sun, H. Qi, S. Lyu, Celeb-df: A large-scale challenging dataset for deepfake forensics, in: *Proceedings of the IEEE/CVF conference on computer vision and pattern recognition*, 2020, pp. 3207–3216.
- [26] A. Rossler, D. Cozzolino, L. Verdoliva, C. Riess, J. Thies, M. Nießner, Faceforensics++: Learning to detect manipulated facial images, in: *Proceedings of the IEEE/CVF international conference on computer vision*, 2019, pp. 1–11.
- [27] N. Dufour, A. Gully, Contributing data to deepfake detection research (Sep 2019).
URL <https://research.google/blog/contributing-data-to-deepfake-detection-research/>
- [28] L. Li, J. Bao, H. Yang, D. Chen, F. Wen, Faceshifter: Towards high fidelity and occlusion aware face swapping, *arXiv preprint arXiv:1912.13457* (2019).
- [29] Y. Li, M.-C. Chang, S. Lyu, In ictu oculi: Exposing ai generated fake face videos by detecting eye blinking, *arXiv preprint arXiv:1806.02877* (2018).
- [30] B. Dolhansky, The deepfake detection challenge (dfdc) preview dataset, *arXiv preprint arXiv:1910.08854* (2019).
- [31] B. Dolhansky, J. Bitton, B. Pflaum, J. Lu, R. Howes, M. Wang, C. C. Ferrer, The deepfake detection challenge (dfdc) dataset, *arXiv preprint arXiv:2006.07397* (2020).

- [32] J. Deng, W. Dong, R. Socher, L.-J. Li, K. Li, L. Fei-Fei, Imagenet: A large-scale hierarchical image database, in: 2009 IEEE conference on computer vision and pattern recognition, Ieee, 2009, pp. 248–255.
- [33] S. G. Mallat, A theory for multiresolution signal decomposition: the wavelet representation, *IEEE transactions on pattern analysis and machine intelligence* 11 (7) (1989) 674–693.
- [34] T. Guo, T. Zhang, E. Lim, M. Lopez-Benitez, F. Ma, L. Yu, A review of wavelet analysis and its applications: Challenges and opportunities, *IEE Access* 10 (2022) 58869–58903.
- [35] M. Sandler, A. Howard, M. Zhu, A. Zhmoginov, L.-C. Chen, Mobilenetv2: Inverted residuals and linear bottlenecks, in: Proceedings of the IEEE conference on computer vision and pattern recognition, 2018, pp. 4510–4520.
- [36] V.-T. Hoang, K.-H. Jo, Practical analysis on architecture of efficientnet, in: 2021 14th International Conference on Human System Interaction (HSI), IEEE, 2021, pp. 1–4.
- [37] J. Hu, L. Shen, G. Sun, Squeeze-and-excitation networks, in: Proceedings of the IEEE conference on computer vision and pattern recognition, 2018, pp. 7132–7141.
- [38] P. Ramachandran, B. Zoph, Q. V. Le, Swish: a self-gated activation function, *arXiv preprint arXiv:1710.05941* 7 (1) (2017) 5.
- [39] H. Touvron, M. Cord, M. Douze, F. Massa, A. Sablayrolles, H. Jégou, Training data-efficient image transformers & distillation through attention, in: International conference on machine learning, PMLR, 2021, pp. 10347–10357.
- [40] A. Dosovitskiy, An image is worth 16x16 words: Transformers for image recognition at scale, *arXiv preprint arXiv:2010.11929* (2020).
- [41] A. Vaswani, Attention is all you need, *Advances in Neural Information Processing Systems* (2017).
- [42] I. Radosavovic, R. P. Kosaraju, R. Girshick, K. He, P. Dollár, Designing network design spaces, in: Proceedings of the IEEE/CVF conference on computer vision and pattern recognition, 2020, pp. 10428–10436.

- [43] Z. Liu, H. Mao, C.-Y. Wu, C. Feichtenhofer, T. Darrell, S. Xie, A convnet for the 2020s, in: Proceedings of the IEEE/CVF conference on computer vision and pattern recognition, 2022, pp. 11976–11986.
- [44] K. He, X. Zhang, S. Ren, J. Sun, Deep residual learning for image recognition, in: Proceedings of the IEEE conference on computer vision and pattern recognition, 2016, pp. 770–778.
- [45] Z. Liu, Y. Lin, Y. Cao, H. Hu, Y. Wei, Z. Zhang, S. Lin, B. Guo, Swin transformer: Hierarchical vision transformer using shifted windows, in: Proceedings of the IEEE/CVF International Conference on Computer Vision (ICCV), 2021, pp. 10012–10022.
- [46] J. L. Ba, J. R. Kiros, G. E. Hinton, Layer normalization, arXiv preprint arXiv:1607.06450 (2016).
- [47] D. Hendrycks, K. Gimpel, Gaussian error linear units (gelus), arXiv preprint arXiv:1606.08415 (2016).
- [48] O. Poursaeed, I. Katsman, B. Gao, S. Belongie, Generative adversarial perturbations, in: Proceedings of the IEEE conference on computer vision and pattern recognition, 2018, pp. 4422–4431.
- [49] I. J. Goodfellow, J. Shlens, C. Szegedy, Explaining and harnessing adversarial examples, arXiv preprint arXiv:1412.6572 (2014).
- [50] P. Neekhara, B. Dolhansky, J. Bitton, C. C. Ferrer, Adversarial threats to deepfake detection: A practical perspective, in: Proceedings of the IEEE/CVF Conference on Computer Vision and Pattern Recognition (CVPR) Workshops, 2021, pp. 923–932.
- [51] A. Gandhi, S. Jain, Adversarial perturbations fool deepfake detectors, in: 2020 International Joint Conference on Neural Networks (IJCNN), 2020, pp. 1–8. doi:10.1109/IJCNN48605.2020.9207034.
- [52] K. Simonyan, Very deep convolutional networks for large-scale image recognition, arXiv preprint arXiv:1409.1556 (2014).
- [53] J. Xu, Y. Pan, X. Pan, S. Hoi, Z. Yi, Z. Xu, Regnet: self-regulated network for image classification, IEEE Transactions on Neural Networks and Learning Systems 34 (11) (2022) 9562–9567.

- [54] C. Szegedy, V. Vanhoucke, S. Ioffe, J. Shlens, Z. Wojna, Rethinking the inception architecture for computer vision, in: Proceedings of the IEEE Conference on Computer Vision and Pattern Recognition (CVPR), 2016.
- [55] G. Huang, Z. Liu, L. Van Der Maaten, K. Q. Weinberger, Densely connected convolutional networks, in: Proceedings of the IEEE conference on computer vision and pattern recognition, 2017, pp. 4700–4708.
- [56] S. Xie, R. Girshick, P. Dollar, Z. Tu, K. He, Aggregated residual transformations for deep neural networks, in: Proceedings of the IEEE Conference on Computer Vision and Pattern Recognition (CVPR), 2017.
- [57] F. Chollet, Xception: Deep learning with depthwise separable convolutions, in: Proceedings of the IEEE conference on computer vision and pattern recognition, 2017, pp. 1251–1258.
- [58] G. Sharir, A. Noy, L. Zelnik-Manor, An image is worth 16x16 words, what is a video worth? (2021). [arXiv:2103.13915](https://arxiv.org/abs/2103.13915)
URL <https://arxiv.org/abs/2103.13915>
- [59] S. Mehta, M. Rastegari, Mobilevit: Light-weight, general-purpose, and mobile-friendly vision transformer (2022). [arXiv:2110.02178](https://arxiv.org/abs/2110.02178)
URL <https://arxiv.org/abs/2110.02178>
- [60] L. Van der Maaten, G. Hinton, Visualizing data using t-sne., Journal of machine learning research 9 (11) (2008).
- [61] H. H. Nguyen, J. Yamagishi, I. Echizen, Use of a capsule network to detect fake images and videos, arXiv preprint arXiv:1910.12467 (2019).
- [62] P. Korshunov, S. Marcel, Deepfakes: a new threat to face recognition? assessment and detection, arXiv preprint arXiv:1812.08685 (2018).
- [63] D. Afchar, V. Nozick, J. Yamagishi, I. Echizen, Mesonet: a compact facial video forgery detection network, in: 2018 IEEE international workshop on information forensics and security (WIFS), IEEE, 2018, pp. 1–7.
- [64] Y. Li, S. Lyu, Exposing deepfake videos by detecting face warping artifacts, arXiv preprint arXiv:1811.00656 (2018).